






Article

Corrosion Resistance of Hard Coat Anodized AA 6061 in Citric–Sulfuric Solutions

José Cabral-Miramontes ¹, Citlalli Gaona-Tiburcio ¹, Francisco Estupinán-López ¹,
María Lara-Banda ¹, Patricia Zambrano-Robledo ¹, Demetrio Nieves-Mendoza ²,
Erick Maldonado-Bandala ², José Chacón-Nava ³ and Facundo Almeraya-Calderón ^{1,*}

¹ Universidad Autónoma de Nuevo León, FIME-Centro de Investigación e Innovación en ingeniería Aeronáutica (CIIIA), Av. Universidad s/n, Ciudad Universitaria, 66455 San Nicolás de los Garza, N.L., Mexico; jose.cabralmr@uanl.edu.mx (J.C.-M.); citlalli.gaonatbr@uanl.edu.mx (C.G.-T.); francisco.estupinanlp@uanl.edu.mx (F.E.-L.); marialarabanda@yahoo.com.mx (M.L.-B.); patricia.zambranor@uanl.edu.mx (P.Z.-R.)

² Universidad Veracruzana, Facultad de Ingeniería Civil, 91000 Xalapa, Mexico; dneieves@uv.mx (D.N.-M.); eemalban@gmail.com (E.M.-B.)

³ Centro de Investigación en Materiales Avanzados (CIMAV), Miguel de Cervantes 120, Complejo Industrial Chihuahua, 31136 Chihuahua, Mexico; jose.chacon@cimav.edu.mx

* Correspondence: falmeraya.uanl.ciiia@gmail.com

Received: 15 May 2020; Accepted: 24 June 2020; Published: 26 June 2020



Abstract: Aluminum is a material widely used in aeronautical and transport industries due to its excellent mechanical and corrosion resistance properties. Unfortunately, aluminum alloys are susceptible to corrosion, which limits their use in some corrosive environments. The aim of this work is to characterize hard coat film fabricated by anodizing in a citric–sulfuric acid system using electrochemical techniques. The anodization process was carried out using an aluminum alloy AA 6061 anodization bath: a mix of citric and sulfuric acid solutions were used. For the anodizing process, two current densities were used, 1 and 7.2 A·cm⁻². Anodized specimens obtained under different conditions were exposed to a 3.5 wt.% NaCl solution, and their electrochemical behavior was studied by electrochemical impedance spectroscopy (EIS) and cyclic potentiodynamic polarization (CPP) according to ASTM G106-15 and ASTM G5-13, respectively. Scanning electron microscopy (SEM) was employed to determinate the morphology and thickness of coatings. The results showed improved corrosion resistance in 6061 aluminum anodized in citric–sulfuric acid electrolyte compared to those anodized in sulfuric acid solution.

Keywords: anodized; aluminum; corrosion; citric acid; electrochemical impedance spectroscopy

1. Introduction

Aluminum and its alloys are widely used in different industries, such as construction, machinery, equipment and transportation. When these alloys are exposed to the atmosphere, a thin aluminum oxide layer of 2 to 4 nm thickness naturally forms on the surface [1–3]. This natural oxide layer imparts improved hardness and excellent corrosion resistance characteristics to aluminum in certain atmospheric and chemical environments [4]. Anodizing is a surface treatment widely used for aluminum alloys due to its reasonable costs compared to the benefits it can offer in terms of enhanced corrosion resistance and mechanical, functional and aesthetic properties. The anodizing process involves first aluminum metal oxidation (Equation (1)) and its subsequent reaction with water to form alumina (Equation (2)) [5].





Anodic aluminum oxide films can be generated by the anodization of aluminum in aqueous electrolytes. Some researchers have shown that the properties of anodizing films can be tuned by changing anodizing conditions. In this way, outer porous layers with a possible ordered pattern [6,7], good wear and corrosion resistance [8,9], and colored surfaces can be obtained [10,11]. Usually, alumina nanostructures are manufactured by an electrochemical process in which the pores grow perpendicularly to a flat surface in a hexagonal structure in the form of a highly ordered honeycomb [12]. The characteristics of alumina films, such as pore diameters and corrosion resistance, depend largely on the electrolyte, current density and duration of the anodizing process [13]. Anodization can be achieved in a variety of electrolytes [14–16]. The electrolytes can be classified into the following three groups: inorganic acids, organic carboxylic acids and organic cyclic oxocarbonic acids [17]. The first group is the most widely used due to its low cost, compared to the electrolytes of the other two groups, and is made up of sulfuric, selenic, chromic and phosphoric acids [18–21]. Group two is comprised of oxalic, malonic and citric organic acids. The presence of carboxylic acid groups allows the formation of complexes with trivalent aluminum and, hence, imparts chemical stability to the coatings [19]. Finally, cyclic oxocarbonic acids, including squaric acid ($\text{C}_4\text{H}_2\text{O}_4$) with a four-membered ring, croconic acid ($\text{C}_5\text{H}_2\text{O}_5$) with a five-membered ring and rhodizonic acid ($\text{C}_6\text{H}_2\text{O}_6$) with a six-membered ring, have recently been reported as useful electrolytes for the formation of porous oxide films and, despite being expensive, provide excellent properties to aluminum, which makes them impractical for use on an industrial scale [22]. Depending on the type of electrolyte used, the growth of the alumina film can be carried out under different conditions, and its porosity and structure characteristics will change depending upon the process variables used, i.e., current density, acid concentration, exposure time etc. Depending on the process chosen, an anodizer can impart to the surface of the aluminum item specific properties as desired, depending on the end use.

According to MIL-A-8625F specifications, anodic coatings can be classified into three types: type I, made with chromic acid and with thicknesses from 1 to 7 μm ; type II, made with sulfuric acid and with thicknesses from 2 to 25 μm ; and type III, hard anodic coatings made with sulfuric acid and other additives such as oxalic and sulfosalicylic acid on aluminum alloys, with an allowable thickness range between 12 and 114 μm , a typical value of 51 μm , and achieving hardness values in the range of 60 to 65 HRC [22–24]. Hard anodizing can increase the tribo-corrosion performance of the components due to the growth of a hard and compact oxide of several tens of microns thickness. Hard anodized aluminum products are characterized by higher resistance to abrasion, improved hardness and a thicker oxide layer [25]. Some alternatives to sulfuric acid for anodizing have recently been used which, although less dangerous than chromic acid, are still dangerous chemicals to be handled, with worrisome environmental effects [26–28].

In recent years attempts has been made to perform type III hard anodizing by adding different organic acids to increase the stability and complexity of the anodized coating structure [29,30]. One of the organic acids used as an additive is citric acid, which is used for its capacity to form complexes with trivalent aluminum. The formation of aluminum complexes with organic molecules is one of the most common additive mechanisms. In this case, the reaction of hard-ion carboxylates with trivalent aluminum cations will readily form complexes that result in insoluble metal soaps that are incorporated onto the surface of the anodic coating. Furthermore, it has been stated that at low concentrations additives provide superior surface finishes, process stability and uniform current distribution [31]. Additionally, the use of citric acid is classified by the Environmental Protection Agency-Safer Chemical Ingredient List (EPA-SCIL) as a safer and more environmentally friendly material [32].

The objective of this work was to evaluate the characteristics on the anodizing film generated by the citric-sulfuric acid anodizing system and the effect on the applied current of the anodizing film, especially the electrochemical behavior.

2. Materials and Methods

2.1. Material

The commercial 6061 aluminum alloy in the form of a 50-mm-diameter rod was used; 5-mm-thick discs were cut from the rod and were used for both the anodization and evaluation of anodized samples by electrochemical techniques. The chemical composition of the 6061 aluminum alloy was obtained by X-ray fluorescence (Olympus DELTA XRF, TX, USA).

2.2. Anodizing Process

Prior to anodization, 5-mm-thick discs cut from the AA 6061 alloy were polished using metallographic techniques. Polishing was performed using different silicon carbide abrasives of grades 180, 320, 400 and 600. The anodizing process consisted of pickling for 5 s in 50 wt.% HCl solution, followed by three rinses in deionized water, each of 3 s duration. Anodizing of the 6061 aluminum alloy was carried out using two solutions as the electrolyte: a solution of sulfuric acid (199.04 g/L) and a solution composed of a mixture of citric acid (210.12 g/L) and 98% sulfuric acid (5 mL/L). A material with a nobler behavior than the 6061 aluminum alloy was used as a cathode; in this case, a lead bar was utilized. The current generator used was a Model XLN30052-GL High Power Programmable DC Power Supply (CA, USA) with a capacity of 300 volts (V) and 5 amperes (A). The variables employed in our anodizing process were the solutions used as the anodizing electrolyte and the current densities used were 1 and 7.2 A·cm⁻² [24]. All anodizing was carried out in an ice bath at a temperature of 5 °C ± 2 °C for 30 min and with stirring of the solution throughout the process. After anodizing, a rinse was carried out in deionized water for 5 s, followed by sealing in deionized water at 95 °C for 30 min. The effect of hot water sealing was to reduce or eliminate the ability of the coating to absorb dyes by blocking the pores, which also increased the corrosion resistance of the coating. Table 1 shows the samples nomenclature and the variables used in the anodizing process.

Table 1. Process parameters for anodizing and nomenclature of the anodized samples.

Material	Anodizing			Sealing	Nomenclature
	Electrolyte	Current Density (A/cm ²)	Time (min)		
AA 6061	H ₂ SO ₄	1	30	Deionized water at 95 °C for 30 min	SA: (sulfuric acid)/1 A·cm ⁻²
	H ₂ SO ₄	7.2	30		SA: (sulfuric acid)/7.2 A·cm ⁻²
	Citric acid + H ₂ SO ₄	1	30		CA: (citric acid)/1 A·cm ⁻²
	Citric acid + H ₂ SO ₄	7.2	30		CA: (citric acid)/7.2 A·cm ⁻²

2.3. Electrochemical Techniques

A conventional three-electrode cell configuration was used for the electrochemical studies, which consisted of a working electrode (un-anodized AA 6061 and anodized aluminum), a saturated calomel electrode (SCE) and a platinum mesh, which were used as a reference and counter electrode, respectively. Electrochemical measurements were carried out using a Gill-AC potentiostat/galvanostat/ZRA from ACM Instruments (Manchester, UK). Corrosion experiments were performed by immersion of the AA 6061 and anodized aluminum specimens, with an exposed surface area of 1.0 cm², in 3.5 wt.% NaCl solution, at a temperature of 25 °C. The electrochemical techniques of cyclic potentiodynamic polarization (CPP) and electrochemical impedance spectroscopy (EIS) were used to determine the corrosion kinetics of AA 6061 with the anodizing treatment. The CPP was recorded at a sweep rate of 0.06 V/min; a potential scan range was applied between −0.3 and 1.0 V vs. SCE, from the corrosion potential (E_{corr}), using a complete polarization cycle, according to ASTM G5-11 standard [33]. In CPP curves, analysis of the cathodic and anodic branches and the hysteresis curve can yield information about the corrosion process in the system, as well as the corrosion rates. Electrochemical impedance spectroscopy measurements were recorded at the corrosion potential over a frequency range from 1 mHz to 100 kHz, obtaining 10 points per decade and applying 10 mV

RMS amplitude according to ASTM G106-15 standard [34]. The results were interpreted through the development of typical impedance models for the electrode surface and curve fitting based on an equivalent circuit using the Zview Impedance program.

2.4. Microstructural Characterization

Analysis of surface morphology and composition was done using a scanning electron microscope (SEM, Jeol JSM 6510LV, Tokyo, Japan). Observations of the cross-sections micrographs of the sample were also made to determine the thickness of the oxide layer at magnification of 2000 \times , operating at a voltage of 20 kV and a working distance (WD) of 12 mm. The chemical composition of the cross-sections structures was obtained by energy dispersive X-ray spectroscopy (EDS).

3. Results and Discussion

3.1. Chemical Composition

The chemical composition of the material under study obtained by X-ray fluorescence is presented in Table 2. The composition of aluminum corresponds to that presented by different authors [24].

Table 2. Chemical composition of Al 6061 by X-ray fluorescence (wt.%).

Elements	Al	Cu	Mg	Mn	Fe	Si	Zn	Cr	Ti
Content	95.15	0.08	2.14	0.03	0.11	2.14	0.15	0.12	0.08

3.2. Cyclic Potentiodynamic Polarization (CPP)

Figure 1 shows the cyclic potentiodynamic polarization curves realized for the un-anodized AA 6061 and anodized material. The absence of a hysteresis loop during the potential scan in un-anodized AA 6061 and SA (sulfuric acid)/1 A \cdot cm $^{-2}$ means that the localized corrosion did not occur, but it could be a sign of an active surface and general corrosion. The results show a positive hysteresis for the following samples, CA (citric acid)/1 A \cdot cm $^{-2}$ and CA (citric acid)/7A \cdot cm $^{-2}$. This behavior is indicative of localized corrosion on the material surface, and the slow decrease of current density in the reverse scan in positive hysteresis is indicative of difficulty in surface repassivation or stopping the growth of pits.

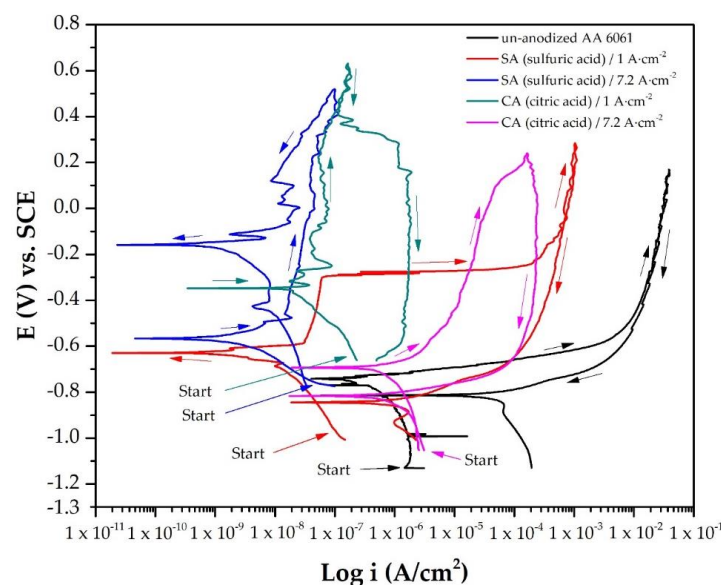


Figure 1. Cyclic potentiodynamic polarization of the un-anodized AA 6061 and samples anodized in 3.5 wt.% NaCl solution.

The behavior of the samples CA (citric acid)/1 A·cm⁻² and CA (citric acid)/7 A·cm⁻² (Figure 1) was observed in AA 2024 and AA 2099, with anodizing treatment evaluated in NaCl [35,36]. Such behavior is attributed to the presence of Cl⁻ ions in the solution [37,38]. The sample anodized only with sulfuric acid and a current density of 7.2 A·cm⁻² (SA (sulfuric acid)/7.2 A·cm⁻²) presented a negative hysteresis cycle, indicating uniform corrosion. In this sample, active–passive transition potential was more noble than corrosion potential (E_{corr}). This occurred for alloys that are susceptible to passivation and hence are able to restore the damaged oxide film or the alloys that are not susceptible to pitting corrosion [39].

Regarding the corrosion potential of the different samples, an increase in the corrosion potential of the anodized samples in sulfuric acid solution can be observed, presenting potentials of around -0.629 V vs. SCE in the sample SA (sulfuric acid)/1 A·cm⁻² and -0.566 V vs. SCE in the sample SA (sulfuric acid)/7.2 A·cm⁻² (Table 3). However, the corrosion potential of the CA (citric acid)/1 A·cm⁻² sample anodized with the citric–sulfuric acid solution presented more noble potentials of around -0.343 V vs. SCE.

Table 3. Electrochemical parameters using cyclic potentiodynamic polarization of AA 6061 and anodized samples in 3.5 wt.% NaCl solution.

Sample	E_{corr} (V vs. SCE)	E_{pit} (V vs. SCE)	E (Anodic to Cathodic Transition) (V vs. SCE)	i_{pass} (nA/cm ²)	i_{corr} (nA/cm ²)
Un-anodized AA 6061	-0.745	-0.745	-0.813	-	156
SA (sulfuric acid)/1 A·cm ⁻²	-0.629	-0.297	-0.844	52.2	22.2
SA (sulfuric acid)/7.2 A·cm ⁻²	-0.566	-	-0.158	42.9	5.93
CA (citric acid)/1 A·cm ⁻²	-0.343	-	-0.659	65.2	17.0
CA (citric acid)/7.2 A·cm ⁻²	-0.693	-0.693	-0.816	-	2620

Only the CA (citric acid)/7.2 A·cm⁻² sample presented corrosion potentials similar to the corrosion potential of the non-anodized material of -0.693 V vs. SCE (Table 3). This may be indicative that although the aluminum oxide layer is formed in the citric–sulfuric acid solution, it does not possess protective characteristics, such as the layers generated in sulfuric acid solution. In addition, it may be due to the porous surface generated during anodization in citric–sulfuric acid solution.

The samples (un-anodized AA 6061 and anodized sample) did not present protection or repassivation potential (E_{Rep}), which is indicative of pitting corrosion, since the potential for anodic to cathodic transition was lower in all cases than the corrosion potential (E_{corr}). For the non-anodized 6061 alloy and CA (citric acid)/7.2 A·cm⁻², the pitting potential (E_{pit}) coincided with the corrosion potential (E_{corr}), which occurred when there was an oxide film on the material surface prior to the polarization. Due to the intersection of cathodic branch with the transpassive region of anodic branch, the value of the pitting potential is the same as the corrosion potential [40,41]. These results are presented in Table 3.

In relation to the effect of the current applied in sulfuric acid solution, it was observed that the sample anodized with 1 A/cm² (SA (sulfuric acid)/1 A·cm⁻²) had a higher current demand in the anodic section of the CPP and a higher passivation current density (i_{pass}), greater than the anodized sample with 7.2 A/cm² (SA (sulfuric acid)/7.2 A·cm⁻²), with both values being 52.2 and 42.9 nA/cm², respectively. This represents the formation of a more stable aluminum oxide film with better properties in the sample made with a higher current, in this case 7.2 A/cm² (see Table 3). In the case of the samples anodized in the citric–sulfuric acid solution, both samples presented similar behaviors in the hysteresis, presenting positive hysteresis (Figure 1).

The anodized sample in the citric–sulfuric acid solution with an anodizing current density of 1 A/cm² had a passivation current density (i_{pass}) of 65.2 nA/cm², while the anodized sample with 7 A/cm² did not show passive behavior. Instead, a considerable current demand was observed in the anodic branch. This behavior was due to the penetration of ions Cl⁻ through the porous oxide layer on the surface, which can also attack the barrier layer. The reference sample, AA 6061 alloy, presented a current demand during the entire cyclic potentiodynamic polarization, and it did not tend

to passivation. This behavior is indicative that the corrosion process was caused by pitting on the surface of this material (Table 3) [42].

Samples SA (sulfuric acid)/1 A·cm⁻², SA (sulfuric acid)/7.2 A·cm⁻² and CA (citric acid)/1 A·cm⁻² presented higher corrosion potentials (E_{corr}) and lower corrosion current densities (i_{corr}), indicating that with these anodizing conditions the corrosion resistance of AA 6061 aluminum alloy was increased.

For the samples of SA (sulfuric acid)/7.2 A·cm⁻² and CA (citric acid)/1 A·cm⁻², the protective layer formed during anodizing hindered the entry of Cl⁻ ions into the pores of the films. This most positive corrosion potential (E_{corr}) was from -0.566 and -0.343 V, and the smallest corrosion current density (i_{corr}) was in the order of nanoamperes/cm² (1×10^{-9} amperes), which indicate a better corrosion resistance with those conditions.

3.3. Electrochemical Impedance Spectroscopy (EIS)

Figure 2a shows the Nyquist plot obtained for the un-anodized and anodized samples in sulfuric acid after exposure to the 3.5 wt.% NaCl electrolyte. The un-anodized specimens show a capacitive loop across the whole frequency range, and for the anodized SA (sulfuric acid/1 A·cm⁻²) and SA (sulfuric acid/7.2 A·cm⁻²) there is a high-frequency semi-circle and capacitive behavior at lower frequencies, which correspond to the characteristics of the porous layer and the barrier layer, respectively. In a similar way, Figure 3a shows the Nyquist plot obtained for the un-anodized and anodized samples in citric-sulfuric acid mixture after exposure to the 3.5 wt.% NaCl electrolyte. In this case, the CA (7.2 A cm⁻²) specimens show a capacitive loop across the entire frequency range, and for the un-anodized sample and CA (citric acid/1 A·cm⁻²) the high-frequency range of the diagram reflects the porous layer characteristics, while the low-frequency range characterizes the barrier layer properties.

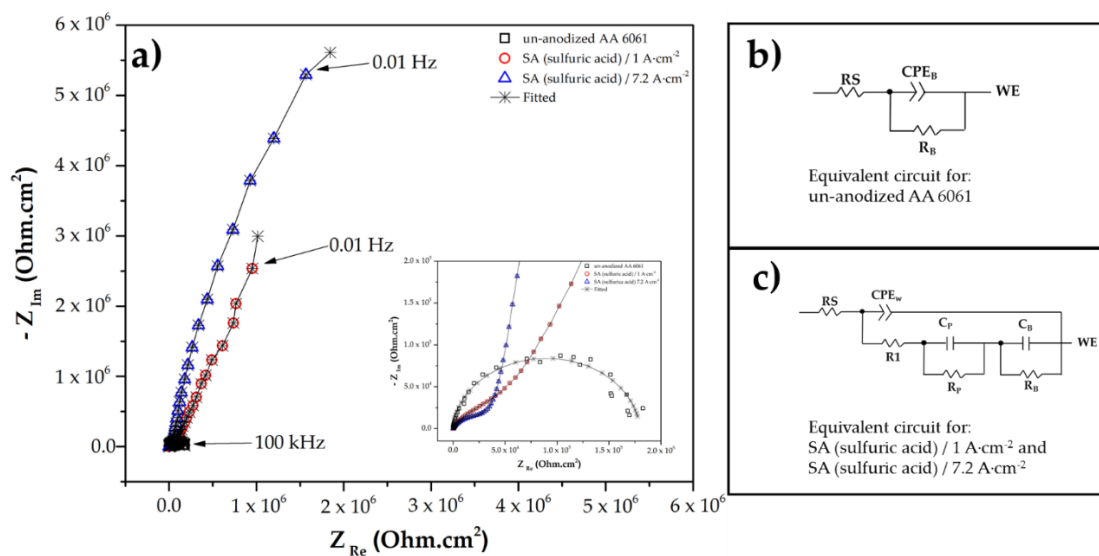


Figure 2. (a) Nyquist diagrams for the un-anodized AA 6061 and samples anodized in sulfuric acid evaluated in 3.5 wt.% NaCl solution; (b,c) equivalent circuits.

Several studies have shown that the low-frequency range corresponds to the properties of the barrier layer and the high- and medium-frequency ranges reflect the properties of the porous layer [43–45]. It has been mentioned previously by some authors that the anodic film on aluminum consists of a very thin compact barrier layer and a thicker porous layer, and that the latter layer is composed of pores and walls of hexagonal-shaped cells. To describe the electrochemical behavior of this system, the thin barrier layer and the porous layer are considered independent of each other [46,47]. To describe these behaviors, several equivalent circuits have been proposed to model the response of porous anodic films [43,48]. It is accepted that different equivalent circuits can model the porous

anodic film; these models are successfully applied to explain the properties of the compact barrier and the porous layers of many materials [44,49–54].

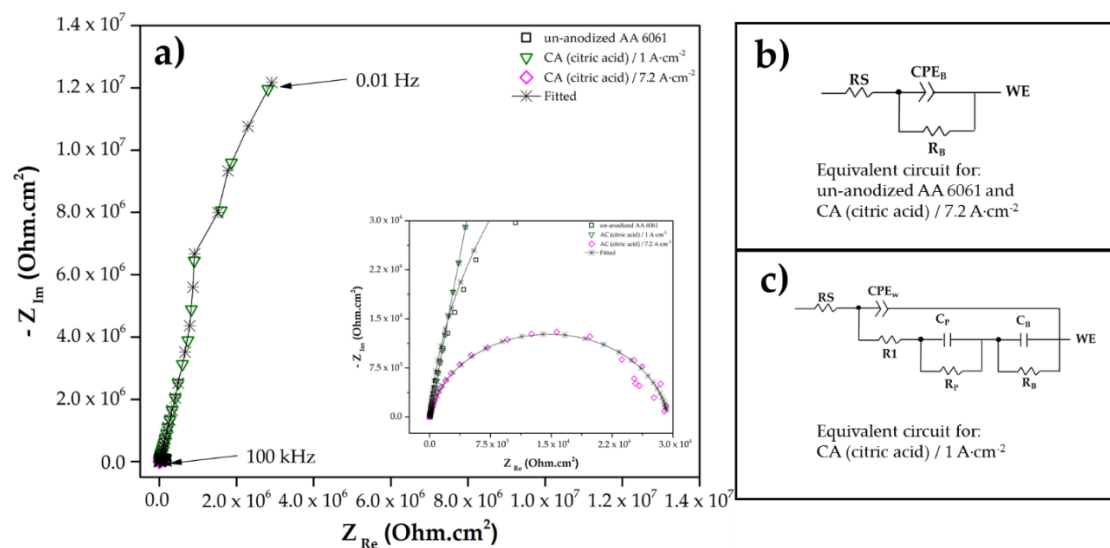


Figure 3. (a) Nyquist diagrams for the un-anodized AA 6061 and samples anodized in citric–sulfuric acid, evaluated in 3.5 wt.% NaCl solution; (b,c) equivalent circuits.

After testing different equivalent circuits for the EIS data obtained, the circuit proposed by Suay et al. [55] gave suitable fits (see Figure 2b,c and Figure 3b,c). In these figures, R_s is the electrolyte resistance, R_B is the barrier layer resistance, CPE_B is the barrier layer constant phase element, n_B is the barrier layer impedance exponent, R_1 is the resistance of ionic pathways in pores and defects, CPE_w is the constant phase element of the cells walls with uniform or nearly uniform dielectric properties, n_w is the cell wall impedance exponent and n_p is the pore barrier impedance exponent. The electrochemical properties of the porous layer are characterized by the capacitance C_p and the resistance R_p , while the properties of the barrier layer are defined by the capacitance R_B and the resistance R_b .

The variation of EIS parameters for the un-anodized AA 6061 and samples anodized under different conditions exposed in 3.5 wt.% NaCl solution is presented in Table 4. The EIS response of the un-anodized AA 6061 sample in the 3.5 wt.% NaCl solution can be represented by the equivalent circuit in Figure 2b, which consists of a resistance R_B and a capacitance C_B in parallel. C_B can be treated as a constant phase element, and because the n_B exponent is 0.94 this means that this constant phase element can be treated as a capacitor. The behavior of anodized SA (sulfuric acid/1 A·cm⁻²) and SA (sulfuric acid/7.2 A·cm⁻²) samples can be represented by the equivalent circuit in Figure 2c. From the values of R_p and R_B in Table 4, it can be seen the beneficial effect of anodizing in sulfuric acid compared with the un-anodized AA 6061 sample. The higher R_p value of the SA (sulfuric acid/1 A·cm⁻²) sample compared to the SA (sulfuric acid/7.2 A·cm⁻²) sample could indicate that the porous layer in the former has a more homogeneous morphology than for the latter.

From Figure 3, it is interesting to note the behavior of the CA (citric acid/1 A·cm⁻²) sample, which had a porous layer R_p value of $3.16 \times 10^9 \Omega\cdot\text{cm}^2$ and a barrier layer R_B value of $522,070 \Omega\cdot\text{cm}^2$ (the highest R_B value measured under all conditions). To some extent, these data and the n_B value obtained indicate the formation of a homogeneous anodized layer.

The value of resistance R_1 (resistance of ionic pathways in pores and defects) can be related to the quality of pore sealing and varies from about 43,337 to 44,223 $\Omega\cdot\text{cm}^2$ for samples anodized with sulfuric acid at 1 A·cm⁻² and 7.2 A·cm⁻², respectively. An R_1 value of 284,410 $\Omega\cdot\text{cm}^2$ was recorded for the CA (citric acid/1 A·cm⁻²) sample. This could be due to a better sealing of pores under this last condition. On the other hand, the higher values of C_B for un-anodized AA 6061 and CA (citric acid/1 A·cm⁻²) samples as compared with other conditions are attributed to a thinner barrier layer.

Last, the better corrosion resistance for the CA (citric acid/1 A·cm⁻²) sample might not be related to a thicker anodized oxide layer. Indeed, this was not the case. Thus, a more homogeneous and organized oxide layer in the CA (citric acid/1 A·cm⁻²) sample probably accounts for its good corrosion resistance. Overall, the EIS data showed better corrosion behavior for the CA (citric acid/1 A·cm⁻²) samples in comparison with the other anodizing conditions.

Table 4. Electrochemical impedance spectroscopy (EIS) data obtained by equivalent electric circuit simulation of the un-anodized AA 6061 and anodized samples at different conditions exposed in 3.5 wt.% NaCl solution.

Samples	R _{sol} (Ω m ²)	CPE _w (μF/cm ²)	n _w	R ₁ (Ω m ²)	C _p (μF/cm ²)	R _p (Ω cm ²)	C _B (μF/cm ²)	n _B	R _B (Ω cm ²)	Error (%)	χ ²
Un-anodized AA 6061	21.58	-	-	-	-	-	6.66	0.94	181,720	<2.58	3 × 10 ⁻²
SA (sulfuric acid)/1 A·cm ⁻²	18.18	0.34	0.80	44,223	1.19	3.72 × 10 ⁹	0.55	1.0	25,487	<2.57	6 × 10 ⁻⁴
SA (sulfuric acid)/7.2 A·cm ⁻²	17.41	0.45	0.71	43,337	1.49	1.00 × 10 ⁹	2.16	1.0	9,199	<2.57	7 × 10 ⁻⁴
CA (citric acid)/1 A·cm ⁻²	27.78	0.86	0.88	284,410	4.82	3.16 × 10 ⁹	3.82	1.0	522,070	<2.60	1 × 10 ⁻²
CA (citric acid)/7.2 A·cm ⁻²	21.81	-	-	-	-	-	15.66	0.90	29,399	<2.57	3 × 10 ⁻²

The combination of anodizing solutions and currents applied in the anodizing process for the two cases presented in this work are indicative that these treatments can be effective against electrolyte penetration, retarding corrosion and degradation of the anodized layer. Therefore, a homogeneous and less porous surface improves the corrosion behavior by restricting the entry of chlorides towards the metallic substrate [56,57].

3.4. SEM Microstructural Analysis

Figure 4 shows the surface morphology obtained by SEM in plan-view for samples anodized with (a) sulfuric acid solution and (b) a mixture of citric–sulfuric acid solution at two currents densities, i.e., 1 and 7.2 A·cm⁻². As can be observed, irrespective of the anodizing solution used, the samples processed using a current density of 7.2 A·cm⁻² presented porosity and superficial cracking (see Figure 4b,d). The anodized samples in both solutions with a current density of 1 A·cm⁻², presented a more homogeneous (less superficial defects) and similar morphology (see Figure 4a,c). In fact, the CA (citric acid)/1 A·cm⁻² sample shows a more regular and smoother surface than that for the SA (sulfuric acid)/1 A·cm⁻² sample, which leads to a better corrosion resistance, since in this condition Cl⁻ ions do not have an easy access path towards the barrier layer and the metallic substrate. For these conditions, the R_p and R_B values from Table 4 confirm the above observations. On the other hand, the sample anodized with citric acid and a current density of 7.2 A·cm⁻² presented the most defective and heterogeneous surface morphology under all conditions, giving the worst performance against corrosion. This type of structure was also observed in a previous study with a mixed tertiary acid anodization process [50]. Other authors have observed similar morphologies on the surface of anodized AA 1050 and AA 2024 T3 aluminum alloys in boric acid solutions [58].

Cross-sectional micrographs obtained by SEM of the anodized AA 6061 alloy under different conditions is shown in Figure 5a–d. A noticeable difference in the thickness of the coatings formed is observed, with the greatest thicknesses being those produced with a current of 7.2 A/cm² in the two anodizing solutions, i.e., 20.7 μm for the anodizing produced in sulfuric acid solution and 14.3 μm for the anodizing produced in the citric–sulfuric acid solution. On these coatings, pores and cracks are visible, in particular for the CA (citric acid)/1 A cm⁻². An important reason for the nucleation of pores and cracks on the anodized layer could be related to the development of thermal stresses caused by the

differences in thermal expansion coefficients of the anodic coating and the metallic substrate during the sealing operation. The observed trend was different from the expected trend of fewer cracks at lower anodization current densities in terms of thermal stresses. Another reason could be related to mechanical stresses induced during the metallographic cross-sections preparation of the samples [59].

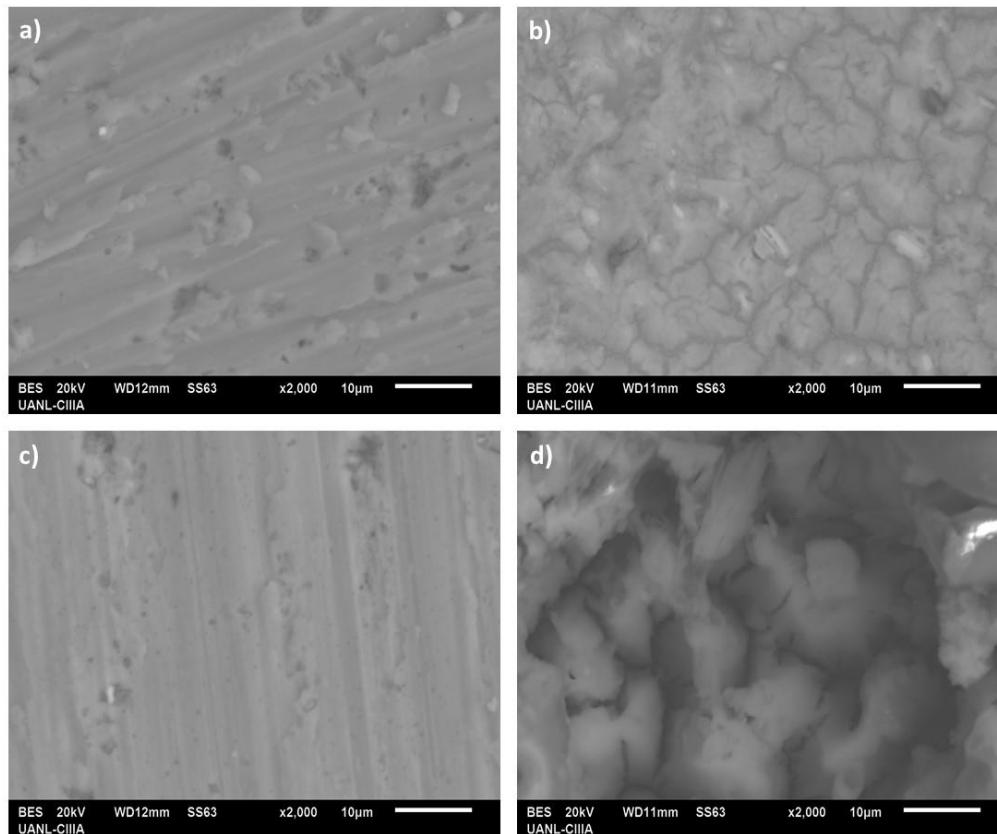


Figure 4. SEM surface morphology micrographs of the samples anodized in sulfuric acid solution and citric–sulfuric acid solution. (a) SA (sulfuric acid)/1 A·cm^{−2}, (b) SA (sulfuric acid)/7.2 A·cm^{−2}, (c) CA (citric acid)/1 A·cm^{−2} and (d) CA (citric acid)/7.2 A·cm^{−2}.

The thinnest anodized coating (3.5 µm) was obtained with the sulfuric acid solution and a current density of 1 A·cm^{−2}, followed by the coating obtained with the citric acid solution and a current density of 1 A·cm^{−2} (7.7 µm). In the former, its good behavior against corrosion could be due to the fact that the porous oxide layer is thick enough and is not being affected by the electrolyte. However, the latter presented the best corrosion performance. This indicates that not only thickness but also other factors such as a more organized and less defective layer structure, are important to explain the behavior found.

In the anodizing process, the coating is created from the surface of the metal. As the coating gets thicker, the current has to pass through the growing layer to reach the clean metal surface. As the coating grows from the bottom up, it may simultaneously be dissolved at the surface. The aggressiveness of the electrolyte is dependent on the properties of the additives in the acid. Thin coatings are produced when the additive in this case citric acid inhibits the dissolution of the oxide coating [31].

In Figure 6, the cross-section of the anodized AA 6061 alloy under different conditions and the element mapping performed by EDS is shown. The cross-section mapping of elements (Figure 6e–h), shows a higher concentration of oxygen (red) in the anodized layer formed in the anodizing solutions and different current densities, which confirms the formation of the anodized layer.

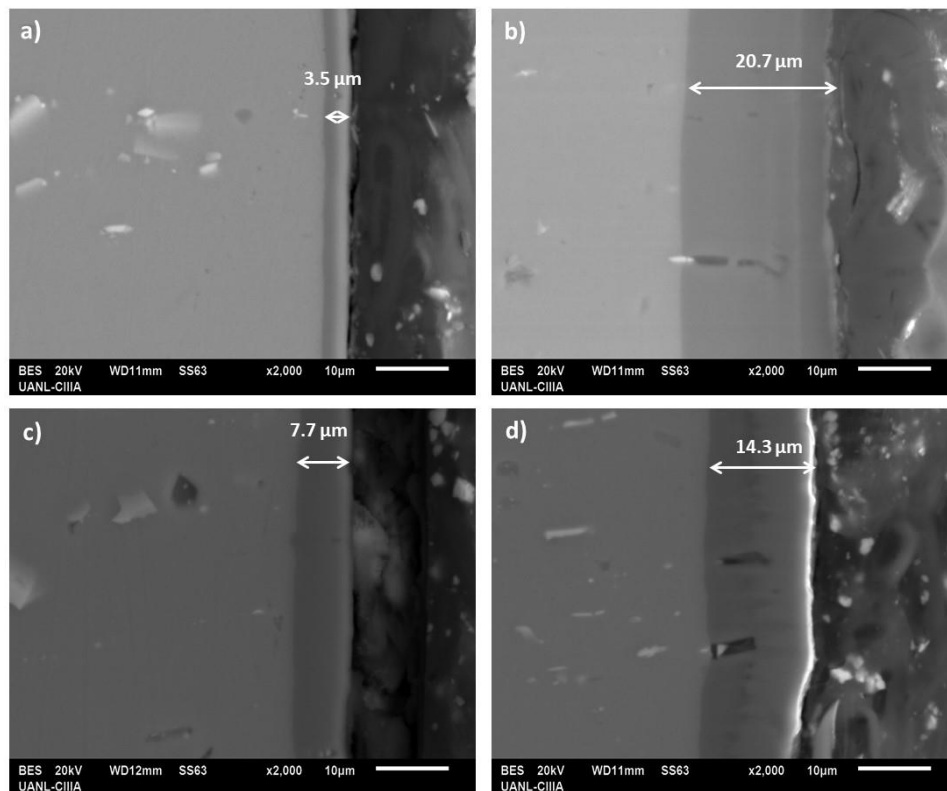


Figure 5. SEM cross-sectional micrographs of the samples anodized in sulfuric acid solution and citric–sulfuric acid solution. (a) SA (sulfuric acid)/1 A·cm⁻², (b) SA (H₂SO₄)/7.2 A·cm⁻², (c) CA (citric acid)/1 A·cm⁻² and (d) CA (citric acid)/7.2 A·cm⁻².

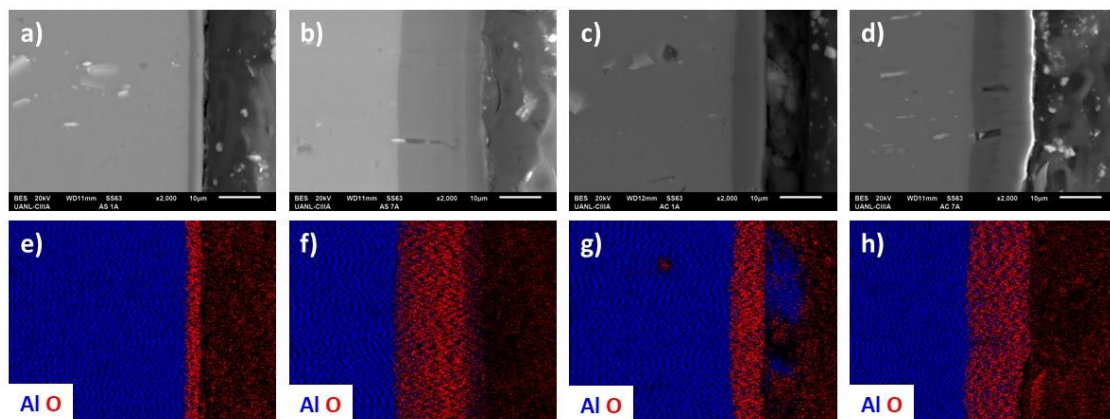


Figure 6. SEM cross-sectional micrographs and element mapping of the anodized samples in sulfuric acid solution and mixture of citric–sulfuric acid solution. (a,e) SA (sulfuric acid)/1 A·cm⁻²; (b,f) SA (sulfuric acid)/7.2 A·cm⁻²; (c,g) CA (citric acid)/1 A·cm⁻² and (d,h) CA (citric acid)/7.2 A·cm⁻².

4. Conclusions

- In this work, samples of AA 6061 were anodized in sulfuric acid and citric–sulfuric acid baths and exposed in a 3.5 wt.% NaCl solution. Their electrochemical behavior was studied by cyclic potentiodynamic polarization and electrochemical impedance spectroscopy.
- In general, cyclic potentiodynamic polarization results indicated that the sample anodized SA (sulfuric acid)/7.2 A·cm⁻² presented negative hysteresis, mainly indicating generalized corrosion, while the rest of the samples presented positive hysteresis indicating a localized corrosion.

- EIS results show that there are two time constants: the first referring to the surface porous layer and the second related to a non-porous and protective barrier layer.
- For the samples anodized with a current density of $1 \text{ A}\cdot\text{cm}^{-2}$, the sample anodized in citric–sulfuric acid solution exhibited the best corrosion resistance, followed by the sample anodized in sulfuric acid solution. The worst performance was observed for the sample anodized in citric–sulfuric acid solution with a current density of $7.2 \text{ A}\cdot\text{cm}^{-2}$.
- SEM observations indicated that the morphology and thickness of the anodic films formed on AA 6061 aluminum in sulfuric acid solution and citric acid–sulfuric acid solution depend upon the current density used. At high-current densities ($7.2 \text{ A}\cdot\text{cm}^{-2}$), there is a considerable increase in the thickness of the anodized layer, compared to anodized samples at low-current densities ($1 \text{ A}\cdot\text{cm}^{-2}$). In the former case, the anodized film presented porosity and cracking, whereas for the latter case, the anodized film was homogeneous and compact.

Author Contributions: Conceptualization—J.C.-M., C.G.-T. and F.A.-C.; methodology—F.E.-L., M.L.-B. and P.Z.-R.; data curation—F.A.-C., E.M.-B., D.N.-M. and J.C.-N.; formal analysis—J.C.-M., J.C.-N. and F.A.-C.; writing—review and editing, J.C.-M., J.C.-N. and F.A.-C. All authors have read and agreed to the published version of the manuscript.

Funding: This research was funded by the Mexican National Council for Science and Technology (CONACYT) of the projects CB 253272 and the Universidad Autónoma de Nuevo León (UANL)—Dirección de Investigación.

Acknowledgments: The authors acknowledge The Academic Body UANL—CA-316 “Deterioration and integrity of composite materials”.

Conflicts of Interest: The authors declare no conflict of interest.

References

1. Evertsson, J.; Bertram, F.; Zhang, F.; Rullik, L.; Merte, L.R.; Shipilin, M.; Soldemo, M.; Ahmadi, S.; Vinogradov, N.; Carlà, F.; et al. The thickness of native oxides on aluminum alloys and single crystals. *Appl. Surf. Sci.* **2015**, *349*, 826–832. [[CrossRef](#)]
2. Nguyen, L.; Hashimoto, T.; Zakharov, D.N.; Stach, E.A.; Rooney, A.P.; Berkels, B.; Thompson, G.E.; Haigh, S.J.; Burnett, T.L. Atomic-scale insights into the oxidation of aluminum. *ACS Appl. Mater. Interfaces* **2018**, *10*, 2230–2235. [[CrossRef](#)] [[PubMed](#)]
3. Dumas, P.; Dubarry-Barbe, J.P.; Riviere, D.; Levy, Y.; Corset, J. Growth of thin alumina film on aluminium at room temperature: A kinetic and spectroscopic study by surface plasmon excitation. *J. Phys. Colloq.* **1983**, *44*, C10-205. [[CrossRef](#)]
4. Wu, Y.; Zhao, W.; Wang, W.; Wang, L.; Xue, Q. Novel anodic oxide film with self-sealing layer showing excellent corrosion resistance. *Sci. Rep.* **2017**, *7*, 1–9. [[CrossRef](#)]
5. Kwolek, P. Hard anodic coatings on aluminum alloys. *Adv. Manuf. Sci. Tech.* **2017**, *41*, 35–46. [[CrossRef](#)]
6. Ono, S.; Saito, M.; Asoh, H. Self-ordering of anodic porous alumina formed in organic acid electrolytes. *Electrochim. Acta* **2005**, *51*, 827–833. [[CrossRef](#)]
7. Lee, W.; Ji, R.; Gosele, U.; Nielsch, K. Fast fabrication of long-range ordered porous alumina membranes by hard anodization. *Nat. Mater.* **2006**, *5*, 741–747. [[CrossRef](#)] [[PubMed](#)]
8. Zhou, X.; Thompson, G.E.; Potts, G. Effects of chromic acid anodizing of aluminum on adhesion and durability of bonded joints. *Trans. Inst. Met. Finish.* **2000**, *78*, 210–214. [[CrossRef](#)]
9. Curioni, M.; Skeldon, P.; Koroleva, E.; Thompson, G.E.; Ferguson, J. Role of tartaric acid on the anodizing and corrosion behavior of AA 2024 T3 aluminum alloy. *J. Electrochem. Soc.* **2009**, *156*, 147–153. [[CrossRef](#)]
10. Wang, H.W.; Skeldon, P.; Thompson, G.E. Tribological enhancement of aluminum by porous anodic films containing solid lubricants of MoS₂ Precursors©. *Tribol. Trans.* **1999**, *42*, 202–209. [[CrossRef](#)]
11. Maejima, M.; Saruwatari, K.; Takaya, M. Friction behavior of anodic oxide film on aluminum impregnated with molybdenum sulfide compounds. *Surf. Coat. Technol.* **2000**, *132*, 105–110. [[CrossRef](#)]
12. Jessensky, O.; Müller, F.; Gösele, U. Self-organized formation of hexagonal pore arrays in anodic alumina. *Appl. Phys. Lett.* **1998**, *72*, 1173–1175. [[CrossRef](#)]

13. Ofoegbu, S.U.; Fábio, A.; Fernandes, F.A.O.; Pereira, A.B. The sealing step in aluminum anodizing: A focus on sustainable strategies for enhancing both energy efficiency and corrosion resistance. *Coatings* **2020**, *10*, 226. [CrossRef]
14. Naoi, K.; Takeda, M.; Kanno, H.; Sakakura, M.; Shimada, A. Simultaneous electrochemical formation of Al₂O₃/polypyrrole layers (I): Effect of electrolyte anion in formation process. *Electrochim. Acta* **2000**, *45*, 3413–3421. [CrossRef]
15. Shang, Y.; Wang, L.; Niu, D.; Liu, Z.; Wang, Y.; Liu, C. Effects of additive for anodizing electrolyte on amodic film of high silicon aluminum alloy. *Int. J. Electrochem. Sci.* **2016**, *11*, 1549–1557.
16. Darwish, S. Anodization of aluminum in phosphate and carbonate solutions. *Corrosion* **1971**, *27*, 266–269. [CrossRef]
17. Kikuchi, T.; Nakajima, D.; Nishinaga, O.; Natsui, S.; Suzuki, R.O. Porous aluminum oxide formed by anodizing in various electrolyte species. *Curr. Nanosci.* **2015**, *11*, 560–571. [CrossRef]
18. Lee, W.; Park, S.J. Porous anodic aluminum oxide: Anodization and templated synthesis of functional nanostructures. *Chem. Rev.* **2014**, *114*, 7487–7556. [CrossRef]
19. Runge, J. *The Metallurgy of Anodizing Aluminum*, 2nd ed.; Springer International Publishing: Chicago, IL, USA, 2018; Volume 65, pp. 149–187.
20. Gabe, D.R. Hard anodizing-what do we mean by hard? *Met. Finish.* **2002**, *100*, 52–58. [CrossRef]
21. Barkey, D.A. *Chemical Process Engineering View of Additives in Aluminum Anodizing*; University of New Hampshire Department of Chemical Engineering: Durham, NH, USA, 2012.
22. Patra, N.; Salerno, M.; Losso, R.; Cingolani, R. Use of unconventional organic acids as Anodization electrolytes for fabrication of porous alumina. *IEEE Nano* **2009**, 567–570.
23. Kikuchi, T.; Nakajima, D.; Kawashima, J.; Natsui, S.; Suzuki, R.O. Fabrication of anodic porous alumina formed in malic acid solution. *Appl. Surf. Sci.* **2014**, *313*, 276–285. [CrossRef]
24. MIL-A-8625F. *Anodic Coatings for Aluminum and Aluminum Alloys*; Departments and Agencies of the Department of Defense: The Pentagon Arlington, VA, USA, 10 September 1993; pp. 1–19.
25. Wojciech, J.S.; Moneta, M.; Norek, M.; Michalska-Domańska, M.; Scarpellini, A.; Salerno, M. The influence of electrolyte composition on the growth of nanoporous anodic alumina. *Electrochim. Acta* **2016**, *211*, 453–460. [CrossRef]
26. Garcia-Vergara, S.J.; Skeldon, P.; Thompson, G.E.; Habazaki, H. A tracer investigation of chromic acid anodizing of aluminium. *Surf. Interface Anal.* **2007**, *39*, 860–864. [CrossRef]
27. Stepniowski, W.J.; Michalska-Domańska, M.; Norek, M.; Czujko, T. Fast Fourier transform based arrangement analysis of poorly organized alumina nanopores formed via self-organized anodization in chromic acid. *Mater. Lett.* **2014**, *117*, 69–73. [CrossRef]
28. Sulfuric Acid. Pubchem.ncbi.nlm.nih.gov. 2020; Retrieved 9 March 2020. Available online: <https://pubchem.ncbi.nlm.nih.gov/compound/Sulfuric-acid#section=EPA-Safer-Chemical> (accessed on 13 March 2020).
29. Schaedel, F.C. Sulfuric/organic electrolytes and total quality improvement (TQI) for present/ future anodizing requirements. *NASF Surf. Technol.* **2017**, *81*, 1–17.
30. Norek, M.; Lazewski, M. Manufacturing of highly ordered porous anodic alumina with conical pore shape and tunable interpore distance in the range of 550 nm to 650 nm. *Mater. Sci. Pol.* **2017**, *35*, 511–518. [CrossRef]
31. Koczera, A.E. The Effects of Carboxylic Acids in Aluminum Anodizing. Ph.D. Thesis, Honors Theses and Capstones, University of New Hampshire, Durham, NH, USA, 2017.
32. Citric Acid. Pubchem.ncbi.nlm.nih.gov. (2020). Retrieved 9 March 2020. Available online: <https://pubchem.ncbi.nlm.nih.gov/compound/Citric-acid#section=EPA-Safer-Chemical> (accessed on 9 January 2020).
33. ASTM G5-11, *Standard Reference Test Method for Making Potentiostatic and Potentiodynamic Anodic Polarization Measurements*; ASTM International: West Conshohocken, PA, USA, 2011.
34. ASTM G106-15, *Standard Practice for Verification of Algorithm and Equipment for Electrochemical Impedance Measurements*; ASTM International: West Conshohocken, PA, USA, 2015.
35. Renaud, A.; Paint, Y.; Lanzutti, A.; Bonnaud, L.; Fedrizzi, L.; Dubois, P.; Poorteman, M.; Olivier, m.G. Sealing Porous anodic layers on AA2024-T3 with a low viscosity benzoxazine resin for corrosion protection in aeronautical applications. *RSC Adv.* **2019**, *9*, 16819–16830. [CrossRef]
36. Cabral, J.; Pedraza, G.K.; Gaona, C.; Zambrano, P.; Poblano, C.A.; Almeraya, F. Coatings characterization of Ni-based alloy applied by HVOF. *Aircr. Eng. Aerosp. Tec.* **2018**, *90*, 336–343. [CrossRef]

37. Lara, M.; Gaona, C.; Zambrano, P.; Cabral, J.; Estupinán, F.; Baltazar, M.; Croche, R.; Vera, E.; Almeraya, F. Corrosion Behaviour of 304 Austenitic, 15–5PH and 17–4PH Passive Stainless Steels in acid solutions. *Int. J. Electrochem. Sci.* **2018**, *13*, 10314–10324. [[CrossRef](#)]
38. Cabral, J.A.; Bastidas, D.M.; Baltazar, M.A.; Zambrano, P.; Bastidas, J.M.; Almeraya, F.; Gaona, C. Corrosion behavior of Zn-TiO₂ and Zn-ZnO electrodeposited coatings in 3.5% NaCl solution. *Int. J. Electrochem. Sci.* **2019**, *14*, 4226–4239. [[CrossRef](#)]
39. Esmailzadeha, S.; Aliofkhaezai, M.; Sarlak, H. Interpretation of cyclic potentiodynamic polarization test results for study of corrosion behavior of metals: A review. *Prot. Met. Phys. Chem. Surf.* **2018**, *54*, 976–989. [[CrossRef](#)]
40. Wang, B.; Liu, J.; Yin, M.; Xiao, Y.; Wang, X.H.; He, J.X. Comparison of corrosion behavior of Al-Mn and Al-Mg alloys in chloride aqueous solution. *Mater. Corros.* **2016**, *67*, 51–59. [[CrossRef](#)]
41. Zaid, B.; Saidi, D.; Hadji, S.; Benzaid, A. Effects of pH and chloride concentration on pitting corrosion of 6061 aluminium alloy. *Corros. Sci. Eng.* **2008**, *50*, 1841–1847. [[CrossRef](#)]
42. Huang, Y.; Shih, H.; Huang, H.; Daugherty, J.; Wu, S.; Ramanathan, S.; Chang, C.; Mansfeld, F. Evaluation of the corrosion resistance of anodized aluminum 6061 using electrochemical impedance spectroscopy (EIS). *Corros. Sci.* **2008**, *50*, 3569–3575. [[CrossRef](#)]
43. Hoar, T.P.; Wood, G.C. The sealing of porous anodic oxide films on aluminium. *Electrochim. Acta* **1962**, *7*, 333–353. [[CrossRef](#)]
44. Hitzig, J.; Junttner, K.; Lorentz, W.J.; Paatsch, W. AC-impedance measurements on porous aluminium oxide films. *Corros. Sci.* **1984**, *24*, 945–952. [[CrossRef](#)]
45. Kwolek, P.; Krupa, K.; Obłój, A.; Kocurek, P.; Wierzbinka, M.; Sieniawski, J. Tribological Properties of the Oxide Coatings Produced onto 6061-T6 Aluminum Alloy in the Hard Anodizing Process. *J. Mater. Eng. Perform.* **2018**, *27*, 3268–3275. [[CrossRef](#)]
46. Sauy, J.J.; Gimenez, E.; Rodriguez, T.; Habbib, K.; Saura, J.J. Characterization of anodized and sealed aluminium by EIS. *Corros. Sci.* **2003**, *45*, 611–624. [[CrossRef](#)]
47. Zhao, X.H.; Zuo, Y.; Zhao, J.M.; Xiong, J.P.; Tang, Y.M. A study on the self-sealing process of anodic films on aluminum by EIS. *Surf. Coat. Technol.* **2006**, *200*, 6846–6853. [[CrossRef](#)]
48. Carangelo, A.; Curioni, M.; Acquesta, A.; Monetta, T.; Bellucci, F. Application of EIS to in situ characterization of hydrothermal sealing of anodized aluminum alloys: Comparison between hexavalent chromium-based sealing, hot water sealing and cerium-based sealing. *J. Electrochem. Soc.* **2016**, *163*, C619–C626. [[CrossRef](#)]
49. Thompson, G.E. Porous anodic alumina: Fabrication, characterization and applications. *Thin Solid Film.* **1997**, *297*, 192–201. [[CrossRef](#)]
50. López, V.; Otero, E.; Bautista, A.; González, J.A. Sealing of anodic films obtained in oxalic acid baths. *Surf. Coat. Technol.* **2000**, *124*, 76–84. [[CrossRef](#)]
51. Bautista, A.; González, J.A.; López, V. Influence of triethanolamine additions on the sealing mechanism of anodised aluminium. *Surf. Coat. Technol.* **2002**, *154*, 49–54. [[CrossRef](#)]
52. Zuo, Y.; Zhao, P.H.; Zhao, J.M. The influences of sealing methods on corrosion behavior of anodized aluminum alloys in NaCl solutions. *Surf. Coat. Technol.* **2003**, *166*, 237–242. [[CrossRef](#)]
53. Snogan, F.; Blanc, C.; Mankowski, G.; Pebere, N. Characterisation of sealed anodic films on 7050 T74 and 2214 T6 aluminium alloys. *Surf. Coat. Technol.* **2002**, *154*, 94–103. [[CrossRef](#)]
54. Dasquet, J.P.; Caillard, U.D.; Conforto, E.; Bonino, J.P.; Bes, R. Investigation of the anodic oxide layer on 1050 and 2024T3 aluminium alloys by electron microscopy and electrochemical impedance spectroscopy. *Thin Solid Film.* **2000**, *371*, 183–190. [[CrossRef](#)]
55. Le Coz, F. Elaboration et Caractérisations de Films Anodiques Hautement Ordonnés, Obtenus à Partir de Substrats D'aluminium. Ph.D. Thesis, Université Toulouse III-Paul Sabatier, Toulouse, France, 2007.
56. Tang, C.W. The Study of Anodic Treatment of Aluminum in Tertiary Mixed Acid after High Temperature Pre-Immersing. Ph.D. Thesis, Tatung University, Taipei, Taiwan, 2005.
57. Gaona-Tiburcio, C.; Montoya, R.M.; Cabral, M.J.A.; Estupiñan, L.F.; Zambrano, R.P.; Orozco, C.R.; Chacon-Nava, J.G.; Baltazar, Z.M.A.; Almeraya-Calderon, F. Corrosion resistance of multilayer coatings deposited by PVD on inconel 718 using electrochemical impedance spectroscopy technique. *Coatings* **2020**, *10*, 521. [[CrossRef](#)]

58. Van Der Linden, B.; Terryn, H.; Vereecken, J. Investigation of anodic aluminium oxide layers by electrochemical impedance spectroscopy. *J. Appl. Electrochem.* **1990**, *20*, 798–803. [[CrossRef](#)]
59. Moutarlier, V.; Gigandet, M.P.; Ricq, L.; Pagetti, J. Electrochemical characterization of anodic oxidation films formed in presence of corrosion inhibitors. *Appl. Surf. Sci.* **2001**, *183*, 1–9. [[CrossRef](#)]



© 2020 by the authors. Licensee MDPI, Basel, Switzerland. This article is an open access article distributed under the terms and conditions of the Creative Commons Attribution (CC BY) license (<http://creativecommons.org/licenses/by/4.0/>).